In situ transport measurements reveal source of mobility enhancement of MoS_2 and $MoTe_2$ during dielectric deposition

Ju Ying Shang,†⁺ Michael J. Moody,†⁺ Jiazhen Chen,‡ Sergiy Krylyuk,§ Albert V. Davydov,§ Tobin J. Marks,‡,† Lincoln J. Lauhon†*

† Department of Materials Science and Engineering, Northwestern University, Evanston, IL 60208, United States
‡ Department of Chemistry, Northwestern University, Evanston, IL 60208, United States
§ Materials Science and Engineering Division, National Institute of Standards and Technology (NIST), Gaithersburg, Maryland 20899, United States

*E-mail: lauhon@northwestern.edu

Abstract

Layered transition metal dichalcogenides (TMDs) and other two-dimensional (2D) materials are promising candidates for enhancing the capabilities of complementary metal-oxide-semiconductor (CMOS) technology. Field-effect transistors (FETs) made with 2D materials often exhibit mobilities below their theoretical limit, and strategies such as encapsulation with dielectrics grown by atomic layer deposition (ALD) have been explored to tune carrier concentration and improve mobility. While molecular adsorbates are known to dope 2D materials and influence charge scattering mechanisms, it is not well understood how ALD reactants affect 2D transistors during growth, motivating in situ or operando studies. Here, we report electrical characterization of MoS_2 and $MoTe_2$ FETs during ALD of MoO_x. The field effect mobility improves significantly within the first five cycles of ALD growth using $Mo(NMe_2)_4$ as the metal−organic precursor and H_2O as the oxidant. Analyses of the in situ transconductance at the growth temperature and ex situ variable temperature transconductance measurements indicate that the majority of the mobility enhancement observed at the beginning of dielectric growth is due to screening of charged impurity scattering by the adlayer. Control experiments show that exposure to only H_2O or O_2 induces more modest and reversible electronic changes in MoTe2 FETs, indicating that negligible oxidation of the TMD takes place during the ALD process. Due to the strong influence of the first <2 nm of deposition, when the dielectric adlayer may be discontinuous and still evolving in stoichiometry, this work highlights the need for further assessment of nucleation layers and initial deposition chemistry, which may be more important than the bulk composition of the oxide itself in optimizing performance and reproducibility.

Keywords: transition metal dichalcogenide, atomic layer deposition, in situ, operando, dielectric screening

Introduction

Layered transition metal dichalcogenides (TMDs) and other two-dimensional (2D) materials are promising candidates for enhancing the capabilities of complementary metal-oxide-semiconductor (CMOS) technology.[1] Although they can exhibit phenomena such as semiconductor-to-metal transitions[2] that allow for novel devices[3,4] and can be scaled more aggressively than conventional CMOS technology, transistors made with 2D materials often exhibit mobilities below their theoretical limit.[5] Furthermore, unintentional doping remains an issue, and conventional substitutional doping can degrade mobility.[6] These challenges have motivated considerable efforts both to improve mobility and also dope 2D materials without degrading mobility.

Beyond improving the starting quality of the 2D crystal itself,[7,8] mobility can be improved with ALD oxide encapsulation.[9] Upon encapsulation, two scattering sources are impacted:[5] remote phonons are introduced from the encapsulation, and charged impurity (CI) scattering may be modified. Conventionally, charged scattering centers of any type, including impurities, adsorbates, and interface traps, are collectively referred to as charged impurities. In a perfect crystal free of defects and contamination, dielectric deposition could in principle decrease mobility because scattering from remote polar phonons would increase.[5] In practice, CI scattering from point defects and interface traps often limits the mobility at room temperature in TMDs[5,9–13] for two reasons. First, screening is reduced in atomically thin semiconductors. Second, typical fabrication methods result in a high density of point defects in the material and charge traps at the substrate interface. In this context, dielectric encapsulation tends to improve the field effect mobility because the increased dielectric constant relative to vacuum[5,14] reduces the Coulomb potential of the CIs. If the dielectric deposition also dopes the TMD, the additional free carriers can also enhance screening of impurities.[5] Prior ex situ studies of devices with different thicknesses of dielectric[15,16] have confirmed expectations that the first few nanometers of dielectric have the greatest impact on mobility. However, it is possible that significant mobility enhancement precedes complete dielectric coverage, and such ex situ studies provide incomplete mechanistic understanding. For example, it has been reported that the density of CIs may also be reduced upon exposure to gaseous reactants,[17] smoothing out the charge distribution. Furthermore, the poorly defined stoichiometry and the instability of very thin nucleation layers in ambient handling or measurement conditions further complicate analysis of this regime in ex situ measurements.

In parallel with efforts to improve mobility, many processes have been identified to dope TMDs, but not all of them maintain or improve mobility. Substitutional doping tends to degrade mobility due to generation of defects that scatter carriers.[6] Charge-transfer doping with molecular adsorbates or metal nanoparticles can increase mobility by increasing free carrier screening,[18] but this doping scheme generally requires additional processing to ensure long-term stability. Charge transfer doping with dielectric encapsulation has the potential to improve mobility[19] and achieve ambient stability[20] at the same time. In

our previous work, MoO_x grown by atomic layer deposition (ALD) was used to dope MoS_2 with electrons or holes.[21] ALD-grown dielectric encapsulation is desirable because it can be performed at temperatures compatible with polymeric materials and can be used on large area substrates.[22] Doping TMDs with dielectric encapsulation has been attributed to transferring of charges due to differences in energy level alignment,[6,19] but some reports have also claimed that diffusion of ions[23] or fixed charges[24] produce the observed changes in carrier concentration. In addition, oxidants used in dielectric growth such as H_2O and O_2 have themselves been reported to dope air-unstable TMDs such as $MoTe_2$.[12,25,26] Such species may adsorb to dope TMDs by charge transfer[18] or in some cases may even oxidize TMDs,[27–29] which changes the electronic band structure.[30] One must therefore ask whether doping more stable (e.g., MoS_2) and less stable (e.g., $MoTe_2$) TMDs by ALD-grown dielectrics occurs via a common mechanism.

In situ monitoring of electronic changes in an FET during ALD growth can provide new insights into the mechanisms that influence mobility enhancement and doping.[31] Transport measurements during the early cycles of dielectric growth should be particularly informative as the semiconductor−dielectric interface is created in the first few growth cycles at a time when each ALD half-cycle can induce significant changes in mobility and carrier concentration. Such conditions cannot be reliably reproduced by ex situ measurements on a series of films of different thicknesses, motiving in situ measurements during film formation.[32] Such measurements could also be considered operando measurements, as the FET is probed under typical electrical operating conditions, but during processing steps that impact the electrical output characteristics.

Here we report *in situ* electronic measurements on MoS_2 and $MoTe_2$ FETs during ALD MoO_x growth. We find that dielectric deposition improves the mobility by factors of 2 to 9. The in situ studies show that most of the enhancement occurs within the first few deposition cycles, implying that dielectric-induced changes in mobility and carrier concentration occur prior to formation of a continuous, stoichiometric, and air-stable dielectric. At longer timescales, gradual decreases in mobility with dielectric thickness are observed, clearly differentiating the two regimes. The change in the temperature dependence of the mobility observed in subsequent ex situ variable-temperature measurements indicates that the improved mobility is predominantly due to screening of charged impurities rather than reaction with or passivation of defects. The submonolayer dielectric regime, which would be difficult to study with ex situ measurements, is of paramount importance to the mobility-enhancing effects of dielectrics and merits further exploration with in situ and operando measurements.

Results and Discussion

In situ measurements were carried out on 2D FETs fabricated from exfoliated MoS_2 and $MoTe_2$ by electron beam lithography (see Experimental Section). As noted above, many prior studies have reported that oxidizing species dope MoS_2 and $MoTe_2$. To provide context for interpreting the evolution of mobility (μ) and carrier concentration (n) during dielectric deposition, we first conducted experiments to isolate the effects of oxidant exposure. $MoTe_2$ FET devices were measured before, during, and after exposure to H_2O, O_2, and O_3 at temperatures and pressures comparable to those used for ALD. FETs were measured in a standard 3-terminal configuration (Figure 1a) in a modified ALD reactor (Figure 1b), and the mobility and carrier concentration were extracted using methods[33,34] described in Supporting Information S1. Measurements, exposures, and growths were performed at 80 °C unless otherwise noted. Transfer curves taken in vacuum immediately before and after oxidant exposure reveal that water and oxygen both have a small but measurable effect on carrier concentration and a negligible effect on field-effect mobility. Mobility varies by less than 1 cm^2/Vs from the starting value of 25 cm^2/Vs, which is negligible considering the ca. 3 cm^2/Vs uncertainty introduced by an increase in hysteresis. After exposure to oxygen, the FET is depleted by 2.2×10^{18} cm^{-3} (a 22% reduction), while after exposure to water, the FET is depleted by 0.6×10^{18} cm^{-3} (a 7% reduction), which is less than 20% of the doping observed with subsequent dielectric encapsulation. This modest shift is likely due to oxygen or water molecules adsorbed on the surface acting as acceptors as previously reported.[24,26] The shift is reversible; baking the device at 180 °C without breaking vacuum restores the original transfer curves, consistent with charge-transfer doping by weakly bound species.

The change in transport can also be monitored in real time via conductivity. As electrons are the majority carriers, the current is proportional to the conductivity $\sigma = ne\mu_e$, where e is the unit charge, and depletion of the n-type channel should manifest as a reduced conductivity. **Figure 1c,d** shows sharp decreases in current (normalized per unit width) upon exposure to pulses of oxygen and water, respectively, with conductivity mostly recovering on the time scale of minutes. Similar to ambient exposure at room temperature,[24,26] changes in electronic properties from exposure to oxygen and water at 80 °C can be reversed with annealing (**Figures 1e,f**). We conclude that, at the ALD growth temperature and the timescale for exposure to ALD reactants (30 min or less), neither oxygen nor water reacts irreversibly with $MoTe_2$. The same behavior can be expected for a more stable TMDs such as MoS_2, where oxidation with oxygen or water on the time scale of tens of minutes requires temperatures of at least 250 °C.[43] Meanwhile, harsher conditions such as annealing at 250 °C reportedly oxidatively dope $MoTe_2$. [24,26] Similarly, our *in situ* measurements during exposure to O_3 (**Supporting Information Section S2**) show that O_3 modifies transport in $MoTe_2$ irreversibly, consistent with prior reports on p-type transport after partial oxidation of $MoTe_2$ to MoO_3.[27] Hence, the studies of changes in doping and mobility during growth reported below are limited to oxygen and water as oxidants.

In situ electrical measurements were carried out on MoS_2 (Figure 2) and $MoTe_2$ (Figure 3) FETs during oxide ALD. Approximately 10 nm of MoO_x was grown in a two-step cycle consisting of alternating doses of $Mo(NMe_2)_4$ and H_2O. Then, approximately 10 nm of Al_2O_3 was grown with alternating doses of $AlMe_3$ and H_2O to ensure ambient stability (MoO_x is not stable in air). Both growths were performed at 80 °C. Low temperature ALD (<100 °C) is useful for promoting initial nucleation by physisorption on relatively inert van der Waals surfaces.[31,35,36] During growth, the channel current was measured continuously at a fixed gate voltage in accumulation (V_g = 55 V unless otherwise noted). Every five cycles, growth was paused to measure the transfer characteristic (V_{DS} set at 0.5 V), enabling the extraction of transport parameters. Figure 2a shows the real-time current density IDS during the first five cycles of MoO_x growth on a MoS_2 FET; the inset shows current (per unit width) during the entire ALD growth. Electrical measurements with corresponding chamber pressure transients are shown in Supporting Information S8 and provide a more detailed view of the changes induced by each precursor species. From each transfer curve (Figure 2b,c), a carrier concentration n (Figure 2d) and intrinsic mobility μ_0 (Figure 2e) were extracted by fitting to a model for FET transfer characteristics in accumulation with a mobility attenuation factor (such as that used in the "Y-function" method[33,34]); details are provided in Supporting Information S1. Both the extracted carrier concentration and mobility sharply increase at the beginning of MoO_x growth: after the first five cycles, for MoS_2, n increased by 60% and μ_0 increased by 2.6 times (calculated in Supporting Information S4). The increase in electron doping with MoO_x deposition is consistent with our previous work, showing that the stoichiometry of MoO_x can be used to control doping in MoS_2.[21] Intriguingly, fully 80% of the mobility change of the entire growth occurs within the first 5 cycles where the dielectric is expected to be less than 1 nm thick.

Significant changes in electrical properties evidently occur even within the first cycle of deposition, during which I_{DS} increases by 12.4 times. Since $\sigma_n = ne\mu_n$, changes in conductivity reflect changes in mobility, carrier concentration, or both. For example, the small downward changes in conductivity with oxidant exposure after the first metal-organic half-cycle are consistent with changes in work function (and thus charge transfer) as the local stoichiometry shifts from oxygen-rich to oxygen-deficient and back again.[21] Considering that the mobility increases 2.6 times during the first 5 cycles, and that the conductivity after one cycle is comparable to the conductivity after 5 cycles, it is likely that a majority of the change in mobility occurs in the first cycle (the electron concentration after one cycle would need to be substantially above its value at 5 cycles for this not to be the case). Qualitatively similar behavior is also seen in the $MoTe_2$ FET measured in parallel. **Figure 3a** shows $MoTe_2$ current density I_{DS} and transfer curves collected every five ALD cycles are shown on linear (**Figure 3b**) and log (**Figure 3c**) scales. Similar to MoS_2, after the first five ALD cycles, there is a sharp increase in *n* (by 50 %, **Figure 3d**) and μ_0 (by 9.4 times, **Figure 3e**) for $MoTe_2$. More than 75 % of the total change in μ_0 occurs in the first five cycles, as observed with

MoS_2. Likewise, I_{DS} increased by 21 times at the end of the first ALD cycle, once again indicating significant changes in transport with less than a monolayer of dielectric. We note that while the large increase in mobility for both MoS_2 and $MoTe_2$ occurs within the first (nominal) nanometer of MoO_x growth, the mobility decreases slightly after ca. 2 nm of growth (**Figures 2e and 3e**). this could suggest that the composition of the dielectric is still evolving. The changes in FET characteristics terminate upon deposition of an Al_2O_3 capping layer (Supporting Information Section S5), which may indicate that alumina prevents diffusion species into or out of the underlying MoO_x.

The carrier mobility is inversely proportional to the scattering rate and effective mass.[37] Since the effective masses of the TMD carriers are not significantly changed by the presence of an oxide,[38] an increase in mobility indicates that carrier scattering has been reduced. Intrinsic phonons, polar surface optical phonons, charged impurities (CI), and atomic (uncharged) defects are each sources of scattering in 2D FETs,[5] and the distinct temperature dependences of these scattering processes may be used to determine the dominant process at a given temperature.[5,37] As discussed in the introduction, intrinsic electron−phonon scattering rates are typically smaller than those of (remote) polar surface optical phonon scattering and charged impurity scattering for typical encapsulated devices at room temperature.[5,9,11−13] Temperature-dependent studies confirm that our unencapsulated devices are indeed limited by CI scattering, as discussed further below. We note that impurities in the semiconductor are not the only type of charged impurity; CI scattering occurs with any large, localized variations in the potential landscape of the semiconductor, which may be due to impurities, adsorbates, or interface traps. Indeed, the adsorption of ALD precursors and the growth of a disordered oxide could potentially add CIs, yet the increase in mobility nonetheless indicates that the overall CI scattering rate is reduced.

One possible explanation for the observed increase in mobility during encapsulation is that the dielectric screens CIs.[5,39] In other words, the dielectric is locally polarized by the Coulomb potential around the CIs, and this polarization in turn reduces or screens the Coulomb potential. However, during the initial deposition cycles studied here, the surface is not yet covered with a continuous oxide, so a model based on a homogeneous dielectric medium of increasing thickness is not appropriate for describing changes at a low cycle number. Indeed, the large increase in current with the first dose of a metal−organic precursor suggests that incomplete coverage of the surface with oxygen-deficient species, perhaps including molecular species, is enough to significantly enhance transport in a TMD. In the absence of a continuous encapsulation layer with a well-defined dielectric constant, we should consider how adsorbed molecules or patchy oxide clusters influence the charge transfer and screening that produce the observed changes in conductivity. Prior work has shown that even modest coverages of molecules (<1/nm^2 for an areal coverage of <10%) can significantly neutralize, displace, or screen CIs.[40,41] Although molecular adsorbates may not form a homogeneous effective medium, they have a finite polarizability and therefore locally screen the Coulomb

potential of CIs in the same manner as continuous dielectrics. Furthermore, our prior work[21] suggests that MoO_x growth under these conditions nucleates without significant intramolecular bonding to the underlying MoS_2, so chemical reactions with the 2D material do not necessarily play a dominant role in the observed changes in mobility and doping. Finally, we note that the possibility of adsorbate-induced modulation of the metal−semiconductor contact resistance was ruled out through control experiments described in Supporting Information S6. This perspective is consistent with the variable-temperature measurements discussed below.

To refine understanding of the microscopic origins of the improvement in mobility, we analyzed the temperature dependence of the mobility (extracted from the transfer curves in Supporting Information S7).[5,9,14,23] The power law exponent γ, where $\mu \sim T^{-\gamma}$, may be used to identify the dominant source of scattering provided the influence of dimensionality is accounted for. For conventional semiconductors where mobility is limited by CI scattering, the mobility typically increases with temperature (a negative γ) due to decreasing interaction times of carriers and CIs with increasing thermal velocity.[37] In contrast, in TMDs with high concentrations of both CIs and free carriers, the mobility decreases with increasing temperature (near room temperature) because the free-carrier screening of CI scattering diminishes.[5,14] In other words, free-carrier screening mitigates CI scattering to increase the mobility overall, but with increasing temperature, this mitigation is reduced, resulting in a mobility that decreases to approach the (lower) CI scattering-limited mobility at higher temperatures. Indeed, the unencapsulated $MoTe_2$ device displays a positive γ of 2.5 ± 0.5 (Figure 4), confirming that mobility is limited by CI scattering, as proposed above based on the observed mobility increase with MoO_x deposition.

After oxide deposition, $\gamma = 0.28 \pm 0.1$, which is consistent with CI screening by a mechanism that is only weakly dependent on temperature. Such a small value is not consistent with phonon scattering, increased free-carrier screening, or a simple reduction in CIs. Phonon scattering would result in a γ of 1.5 or greater, depending on the phonon modes.[5,11] Free carrier screening, as seen in the unencapsulated sample and in theoretical models,[5] results in a steeper temperature dependence ($\gamma > 0.8$) and would not change dramatically due to the small (20−50%) changes in carrier concentration seen here. Passivation alone, i.e., a reduction in the density of CIs, would improve the mobility, but γ would not change. Based on the observed decrease in γ upon encapsulation, we conclude that the influence of dielectric screening, which is largely temperature-independent,[5] has increased relative to these other contributions. While free-carrier screening and optical phonon scattering almost certainly increase, and passivation may occur, their effects on mobility are minor compared to screening by a polarizable medium such as a dielectric or polarizable molecules, which results in a mobility enhancement that is preserved at higher temperatures.

Conclusion

In summary, in situ experiments on TMD FETs encapsulated with ALD oxide dielectrics revealed the disproportionate influence of the initial oxide deposition cycles on device performance. Carrier concentration and mobility both increase dramatically within the first five ALD cycles. We attribute the majority of the increase in mobility to a reduction in CI scattering due to increased dielectric screening of CIs in the early stages of dielectric growth. Further improvements in performance might be realized by optimizing the initial exposure, potentially with conditions or species that differ from the steady-state oxide growth conditions. We note, for example, that seeding layers or oxidation treatments have been used to promote ALD growth of dielectrics[27,42–44] on two dimensional materials but are not necessarily independently optimized for preservation or enhancement of mobility. Further progress in mobility enhancement through encapsulation may be realized via multistep processes that are designed to optimize the interface and first nanometer of the material separately from the bulk of the dielectric. The in situ methodology demonstrated here provides an efficient way to study these and other questions of evolving interfaces and transport in nanoscale electronic devices such as 2D FETs.

Experimental Section

2H-$MoTe_2$ crystals were grown using chemical vapor transport as described in reference[45] and MoS_2 crystals were purchased from SPI Supplies. To fabricate FETs, $MoTe_2$ and MoS_2 crystals were mechanically exfoliated onto 285 nm SiO_2/Si wafers, with degenerately doped Si as the back gate. A standard two-step electron-beam lithography process was used to define thermally evaporated gold contacts. Devices were connected to an ALD compatible custom chip carrier via wedge bonding, which was loaded into the ALD reactor and connected via UHV-grade cabling and feedthroughs (Accu-Glass Products) to Keithley 2400 source-measure units.

In situ measurements on MoS_2 (Figure 2) and $MoTe_2$ (Figure 3) FETs were carried out in a modified Ultratech Savannah S200 with an in situ quartz crystal microbalance (QCM) and an insulated lid under continuous, viscous flow conditions with 20 sccm ultrahigh purity N_2 (99.999%, Airgas) as a purge gas. Degassed HPLC-grade water (Fisher) and ultra-high purity oxygen (99.996%, Airgas) were dosed to achieve partial pressures of 2 Torr in the chamber.

MoO_x was grown at 80 °C in a two-step cycle consisting of a $Mo(NMe_2)_4$ dose, a 30 s purge, a H_2O dose, and a 30 s purge. Following the growth of approximately 10 nm of MoO_x, approximately 10 nm of Al_2O_3 was grown by alternating doses of trimethyl aluminum (Sigma-Aldrich) and H_2O to ensure ambient stability. During growth, the channel current was measured continuously at a fixed gate voltage in accumulation (V_g = 55 V unless otherwise noted). Every five cycles, growth was paused to measure the transfer characteristic

(V_{DS} set at 0.5 V), enabling the extraction of transport parameters. With 20 sccm ultrahigh purity N_2, the reactor pressure during measurement was 0.3 Torr.

Associated content

Supporting Information

The Supporting Information is available free of charge at https://pubs.acs.org/doi/10.1021/acsaelm.0c00085. Analysis of transfer characteristics, ozone exposure experiments, correlated electrical and pressure data, details of mobility changes at early growth, electrical characteristics during deposition of capping layer, ALD with masked FETs, variable-temperature measurements, and list of devices (PDF)

Author Information

Corresponding Author

Lincoln J. Lauhon − Department of Materials Science and Engineering, Northwestern University, Evanston, Illinois 60208, United States; Email: lauhon@northwestern.edu

Authors

Ju Ying Shang − Department of Materials Science and Engineering, Northwestern University, Evanston, Illinois 60208, United States

Michael J. Moody − Department of Materials Science and Engineering, Northwestern University, Evanston, Illinois 60208, United States

Jiazhen Chen − Department of Chemistry, Northwestern University, Evanston, Illinois 60208, United States; orcid.org/0000-0002-9023-3072

Sergiy Krylyuk − Materials Science and Engineering Division, National Institute of Standards and Technology (NIST), Gaithersburg, Maryland 20899, United States

Albert V. Davydov − Materials Science and Engineering Division, National Institute of Standards and Technology (NIST), Gaithersburg, Maryland 20899, United States; orcid.org/0000-0003-4512-2311

Tobin J. Marks − Department of Chemistry and Department of Materials Science and Engineering, Northwestern University, Evanston, Illinois 60208, United States; orcid.org/0000-0001-8771-0141

Acknowledgments

This work was supported in part by the U.S. Department of Commerce, National Institute of Standards and Technology under financial assistance award numbers 70NANB14H012 and 70NANB19H005, and by the NSF via EFRI-1433510 and via the Materials Research Science and Engineering Center (MRSEC) of Northwestern University (NSF DMR-1720139). It made use of the NUFAB, EPIC, and SPID facilities of the NUANCE Center at Northwestern University, which have received support from the Soft and Hybrid Nanotechnology Experimental (SHyNE) Resource (NSF ECCS-154220); the MRSEC program (NSF DMR-1720139) at the Materials Research Center; the International Institute for Nanotechnology (IIN); the

Keck Foundation; and the State of Illinois, through the IIN. M.J.M. gratefully acknowledges support via a 3M Fellowship, as well as from the Ryan Fellowship and the Northwestern University International Institute for Nanotechnology. Disclaimer: Certain commercial equipment, instruments, or materials are identified in this paper to specify the experimental procedure adequately. Such identification is not intended to imply recommendation or endorsement by the National Institute of Standards and Technology, nor is it intended to imply that the materials or equipment identified are necessarily the best available for the purpose.

References

(1) Akinwande, D.; Huyghebaert, C.; Wang, C.-H.; Serna, M. I.; Goossens, S.; Li, L.-J.; Wong, H.-S. P.; Koppens, F. H. L. Graphene and two-dimensional materials for silicon technology. Nature 2019, 573, 507−518.

(2) Wang, Y.; Xiao, J.; Zhu, H.; Li, Y.; Alsaid, Y.; Fong, K. Y.; Zhou, Y.; Wang, S.; Shi, W.; Wang, Y.; Zettl, A.; Reed, E. J.; Zhang, X. Structural phase transition in monolayer MoTe2 driven by electrostatic doping. Nature 2017, 550, 487.

(3) Hou, W.; Azizimanesh, A.; Sewaket, A.; Peña, T.; Watson, C.; Liu, M.; Askari, H.; Wu, S. M. Strain-based room-temperature nonvolatile MoTe2 ferroelectric phase change transistor. Nat. Nanotechnol. 2019, 14, 668−673.

(4) Cho, S.; Kim, S.; Kim, J. H.; Zhao, J.; Seok, J.; Keum, D. H.; Baik, J.; Choe, D.-H.; Chang, K. J.; Suenaga, K.; Kim, S. W.; Lee, Y. H.; Yang, H. Phase patterning for ohmic homojunction contact in MoTe2. Science 2015, 349, 625−628.

(5) Yu, Z.; Ong, Z.-Y.; Li, S.; Xu, J.-B.; Zhang, G.; Zhang, Y.-W.; Shi, Y.; Wang, X. Analyzing the Carrier Mobility in Transition-Metal Dichalcogenide MoS2 Field-Effect Transistors. Adv. Funct. Mater. 2017, 27, 1604093.

(6) Luo, P.; Zhuge, F.; Zhang, Q.; Chen, Y.; Lv, L.; Huang, Y.; Li, H.; Zhai, T. Doping engineering and functionalization of twodimensional metal chalcogenides. Nanoscale Horiz. 2019, 4, 26−51.

(7) Andrzejewski, D.; Marx, M.; Grundmann, A.; Pfingsten, O.; Kalisch, H.; Vescan, A.; Heuken, M.; Kümmell, T.; Bacher, G. Improved luminescence properties of MoS2 monolayers grown via MOCVD: role of pre-treatment and growth parameters. Nanotechnology 2018, 29, 295704.

(8) Kang, K.; Xie, S.; Huang, L.; Han, Y.; Huang, P. Y.; Mak, K. F.; Kim, C.-J.; Muller, D.; Park, J. High-mobility three-atom-thick semiconducting films with wafer-scale homogeneity. Nature 2015, 520, 656.

(9) Radisavljevic, B.; Kis, A. Mobility engineering and a metal−insulator transition in monolayer MoS2. Nat. Mater. 2013, 12, 815− 820.

(10) Ma, N.; Jena, D. Charge Scattering and Mobility in Atomically Thin Semiconductors. Phys. Rev. X 2014, 4, No. 011043.

(11) Yu, Z.; Ong, Z.-Y.; Pan, Y.; Cui, Y.; Xin, R.; Shi, Y.; Wang, B.; Wu, Y.; Chen, T.; Zhang, Y.-W.; Zhang, G.; Wang, X. Realization of Room-Temperature Phonon-Limited Carrier Transport in Monolayer MoS2 by Dielectric and Carrier Screening. Adv. Mater. 2016, 28, 547−552.

(12) Schmidt, H.; Wang, S.; Chu, L.; Toh, M.; Kumar, R.; Zhao, W.; Neto, A. H. C.; Martin, J.; Adam, S.; Özyilmaz, B.; Eda, G. Transport properties of monolayer MoS2 grown by chemical vapor deposition. Nano Lett. 2014, 14, 1909−1913.

(13) Liu, Y.; Wu, H.; Cheng, H.-C.; Yang, S.; Zhu, E.; He, Q.; Ding, M.; Li, D.; Guo, J.; Weiss, N. O.; Huang, Y.; Duan, X. Toward barrier free contact to molybdenum disulfide using graphene electrodes. Nano Lett. 2015, 15, 3030−3034.

(14) Ong, Z.-Y.; Fischetti, M. V. Mobility enhancement and temperature dependence in top-gated single-layer MoS2. Phys. Rev. B 2013, 88, 165316.

(15) Luo, W.; Zhu, M.; Peng, G.; Zheng, X.; Miao, F.; Bai, S.; Zhang, X.-A.; Qin, S. Carrier Modulation of Ambipolar Few-Layer MoTe2 Transistors by MgO Surface Charge Transfer Doping. Adv. Funct. Mater. 2018, 1704539.

(16) Xu, J.; Wen, M.; Zhao, X.; Liu, L.; Song, X.; Lai, P.-T.; Tang, W.-M. Effects of HfO2 encapsulation on electrical performances of few-layered MoS2 transistor with ALD HfO2 as back-gate dielectric. Nanotechnology 2018, 29, 345201.

(17) Li, S.-L.; Tsukagoshi, K.; Orgiu, E.; Samori, P. Charge Transport and Mobility Engineering in Two-Dimensional Transition Metal Chalcogenide Semiconductors. Chem. Soc. Rev. 2015, 45, 1−151.

(18) Zhang, X.; Shao, Z.; Zhang, X.; He, Y.; Jie, J. Surface Charge Transfer Doping of Low-Dimensional Nanostructures toward High- Performance Nanodevices. Adv. Mater. 2016, 28, 10409−10442.

(19) Hu, Z.; Wu, Z.; Han, C.; He, J.; Ni, Z.; Chen, W. Two dimensional transition metal dichalcogenides: interface and defect engineering. Chem. Soc. Rev. 2018, 47, 3100−3128.

(20) Li, Q.; Zhou, Q.; Shi, L.; Chen, Q.; Wang, J. Recent advances in oxidation and degradation mechanisms of ultrathin 2D materials under ambient conditions and their passivation strategies. J. Mater. Chem. A 2019, 7, 4291−4312.

(21) Moody, M. J.; Henning, A.; Jurca, T.; Shang, J. Y.; Bergeron, H.; Balla, I.; Olding, J. N.; Weiss, E. A.; Hersam, M. C.; Lohr, T. L.; Marks, T. J.; Lauhon, L. J. Atomic Layer Deposition of Molybdenum Oxides with Tunable Stoichiometry Enables Controllable Doping of MoS2. Chem. Mater. 2018, 30, 3628−3632.

(22) George, S. M. Atomic Layer Deposition: An Overview. Chem. Rev. 2009, 110, 111−131.

(23) Lee, H. S.; Park, S.; Lim, J. Y.; Yu, S.; Ahn, J.; Hwang, D. K.; Sim, Y.; Lee, J.-H.; Seong, M.-J.; Oh, S.; Choi, H. J.; Im, S. Impact of H-Doping on n-Type TMD Channels for Low-Temperature Band-Like Transport. Small 2019, 15, 1901793.

(24) Qu, D.; Liu, X.; Huang, M.; Lee, C.; Ahmed, F.; Kim, H.; Ruoff, R. S.; Hone, J.; Yoo, W. J. Carrier-Type Modulation and Mobility Improvement of Thin MoTe2. Adv. Mater. 2017, 29, 1606433.

(25) Chen, B.; Sahin, H.; Suslu, A.; Ding, L.; Bertoni, M. I.; Peeters, F. M.; Tongay, S. Environmental Changes in MoTe2 Excitonic Dynamics by Defects-Activated Molecular Interaction. ACS Nano 2015, 9, 5326−5332.

(26) Chang, Y.-M.; Yang, S.-H.; Lin, C.-Y.; Chen, C.-H.; Lien, C.-H.; Jian, W.-B.; Ueno, K.; Suen, Y.-W.; Tsukagoshi, K.; Lin, Y.-F. Reversible and Precisely Controllable p/n-Type Doping of MoTe2 Transistors through Electrothermal Doping. Adv. Mater. 2018, 30, 1706995.

(27) Zheng, X.; Wei, Y.; Deng, C.; Huang, H.; Yu, Y.; Wang, G.; Peng, G.; Zhu, Z.; Zhang, Y.; Jiang, T.; Qin, S.; Zhang, R.; Zhang, X. Controlled Layer-by-Layer Oxidation of MoTe2 via O3 Exposure. ACS Appl. Mater. Interfaces 2018, 10, 30045−30050.

(28) Seo, S.-Y.; Park, J.; Park, J.; Song, K.; Cha, S.; Sim, S.; Choi, S.- Y.; Yeom, H. W.; Choi, H.; Jo, M.-H. Writing monolithic integrated circuits on a two-dimensional semiconductor with a scanning light probe. Nat. Electron. 2018, 1, 512−517.

(29) Pető, J.; Ollár, T.; Vancsó, P.; Popov, Z. I.; Magda, G. Z.; Dobrik, G.; Hwang, C.; Sorokin, P. B.; Tapasztó, L. Spontaneous doping of the basal plane of MoS2 single layers through oxygen substitution under ambient conditions. Nat. Chem. 2018, 10, 1246−1251.

(30) Liu, H.; Han, N.; Zhao, J. Atomistic insight into the oxidation of monolayer transition metal dichalcogenides: from structures to electronic properties. RSC Adv. 2015, 5, 17572−17581.

(31) Jandhyala, S.; Mordi, G.; Lee, B.; Lee, G.; Floresca, C.; Cha, P.-R.; Ahn, J.; Wallace, R. M.; Chabal, Y. J.; Kim, M. J.; Colombo, L.; Cho, K.; Kim, J. Atomic Layer Deposition of Dielectrics on Graphene Using Reversibly Physisorbed Ozone. ACS Nano 2012, 6, 2722−2730.

(32) Qi, D.; Han, C.; Rong, X.; Zhang, X.-W.; Chhowalla, M.; Wee, A. T. S.; Zhang, W. Continuously Tuning Electronic Properties of Few-Layer Molybdenum Ditelluride with in Situ Aluminum Modification toward Ultrahigh Gain Complementary Inverters. ACS Nano 2019, 13, 9464−9472.

(33) Schroder, D. K. Semiconductor Material and Device Characterization; John Wiley & Sons, Inc.: 2006, 489−499.

(34) Xu, Y.; Minari, T.; Tsukagoshi, K.; Chroboczek, J. A.; Ghibaudo, G. Direct evaluation of low-field mobility and access resistance in pentacene field-effect transistors. J. Appl. Phys. 2010, 107, 114507.

(35) Wood, J. D.; Wells, S. A.; Jariwala, D.; Chen, K.-S.; Cho, E.; Sangwan, V. K.; Liu, X.; Lauhon, L. J.; Marks, T. J.; Hersam, M. C. Effective passivation of exfoliated black phosphorus transistors against ambient degradation. Nano Lett. 2014, 14, 6964−6970.

(36) Teich, J.; Dvir, R.; Henning, A.; Hamo, E. R.; Moody, M. J.; Jurca, T.; Cohen, H.; Marks, T. J.; Rosen, B. A.; Lauhon, L. J.; Ismach, A. Light and complex 3D MoS2/graphene heterostructures as efficient catalysts for the hydrogen evolution reaction. Nanoscale 2020, 12, 2715−2725.

(37) Sze, S. M. Physics of Semiconductor Devices; 2nd Ed.; Wiley: New York, 1981.

(38) Biel, B.; Donetti, L.; Ortiz, E. R.; Godoy, A.; Gámiz, F. Tunability of effective masses on MoS2 monolayers. Microelectron. Eng. 2015, 147, 302−305.

(39) Gerber, I. C.; Marie, X. Dependence of band structure and exciton properties of encapsulated WSe2 monolayers on the hBN layer thickness. Phys. Rev. B 2018, 98, 245126.

(40) Worley, B. C.; Haws, R. T.; Rossky, P. J.; Dodabalapur, A. Chemical Understanding of the Mechanisms Involved in Mitigation of Charged Impurity Effects by Polar Molecules on Graphene. J. Phys. Chem. C 2016, 120, 12909−12916.

(41) Worley, B. C.; Kim, S.; Park, S.; Rossky, P. J.; Akinwande, D.; Dodabalapur, A. Dramatic vapor-phase modulation of the characteristics of graphene field-effect transistors. Phys. Chem. Chem. Phys. 2015, 17, 18426−18430.

(42) Kim, H. G.; Lee, H.-B.-R. Atomic Layer Deposition on 2D Materials. Chem. Mater. 2017, 29, 3809−3826.

(43) Azcatl, A.; Kc, S.; Peng, X.; Lu, N.; McDonnell, S.; Qin, X.; de Dios, F.; Addou, R.; Kim, J.; Kim, M. J.; Cho, K.; Wallace, R. M. HfO2 on UV−O3 exposed transition metal dichalcogenides: interfacial reactions study. 2D Mater. 2015, 2, No. 014004.

(44) Walter, T. N.; Kwok, F.; Simchi, H.; Aldosari, H. M.; Mohney, S. E. Oxidation and oxidative vapor-phase etching of few-layer MoS2. J. Vac. Sci. Technol., B: Nanotechnol. Microelectron.: Mater., Process., Meas., Phenom. 2017, 35, No. 021203.

(45) Oliver, S. M.; Beams, R.; Krylyuk, S.; Kalish, I.; Singh, A. K.; Bruma, A.; Tavazza, F.; Joshi, J.; Stone, I. R.; Stranick, S. J.; Davydov, A. V.; Vora, P. M. The structural phases and vibrational properties of Mo1−xWxTe2 alloys. 2D Mater. 2017, 4, No. 045008.

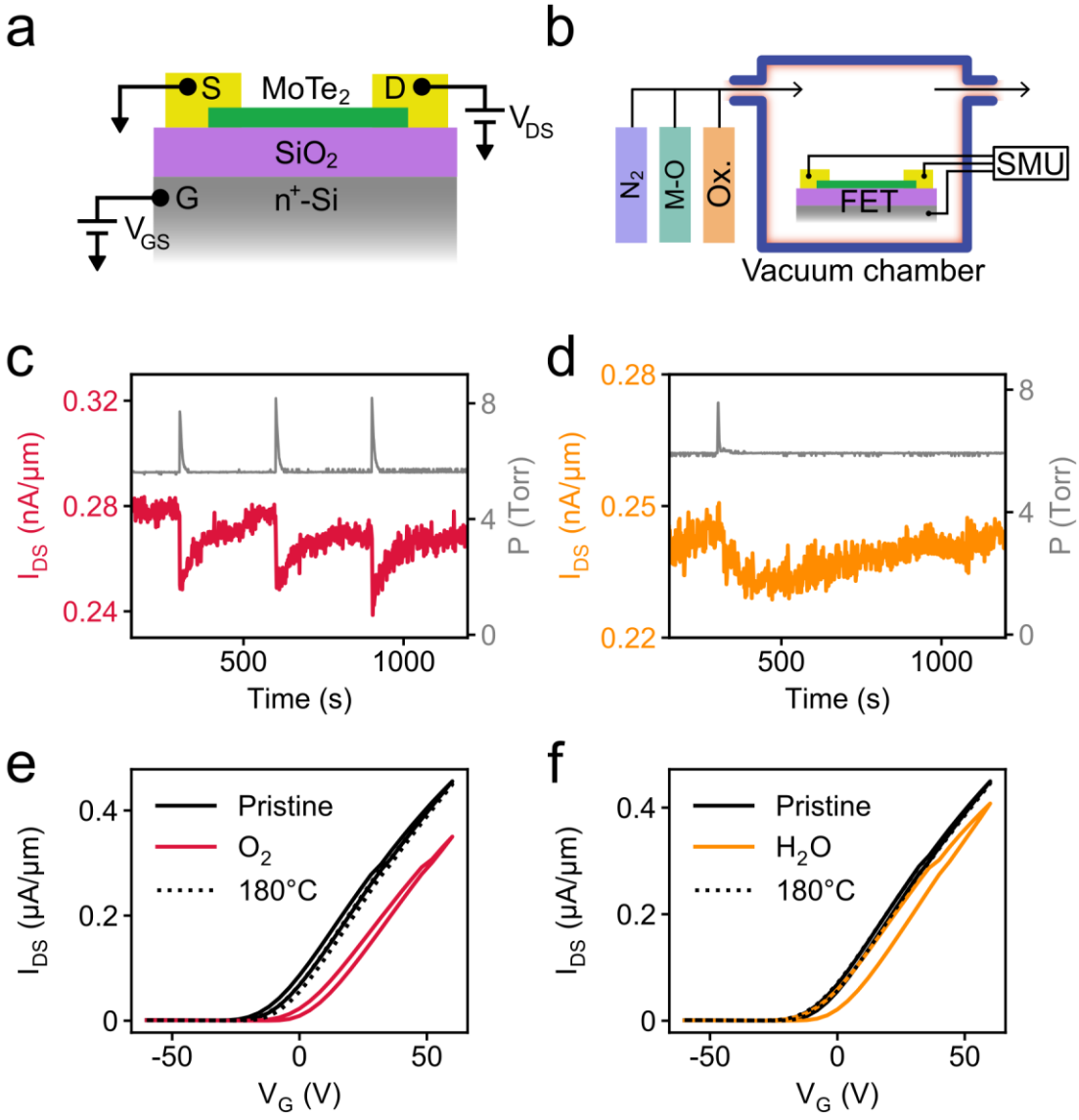

Figure 1. In situ measurements of 2D FETs. (a) Schematic of a backgated FET. (b) Schematic of the modified ALD reactor for in situ measurements. SMU is source-measure unit. (c) Pulsed oxygen and (d) water exposures on $MoTe_2$ at 180 °C with V_G set at 0 V and V_{SD} set at 0.05 V, showing reversible changes with time in current density. Transport characteristics (V_{SD} set at 0.1 V) are reversible with annealing at 180 °C after 30 min exposure to (e) oxygen or (f) water at 80 °C.

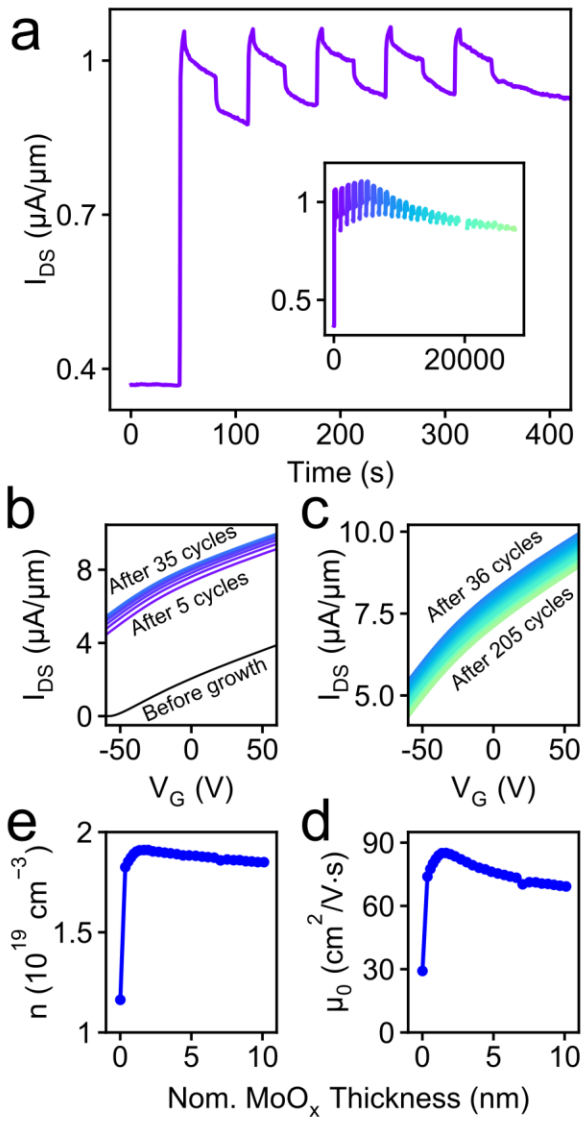

Figure 2. Evolution of electronic properties of MoS_2 during ALD MoO_x growth. (a) Current density IDS during the first five cycles of growth with V_G set at 55 V and V_{SD} set at 0.05 V. Inset: I_{DS} during the entire growth. (b) Consecutive transfer curves collected every five ALD cycle for 35 cycles showing increasing current density (indicated by arrow). (c) Transport characteristics collected for the rest of the growth, during which current density decreases, as indicated by the arrow. (d) Carrier concentration n and (e) intrinsic mobility μ_0 are extracted from (b) and (c), showing significant increase at the beginning of growth.

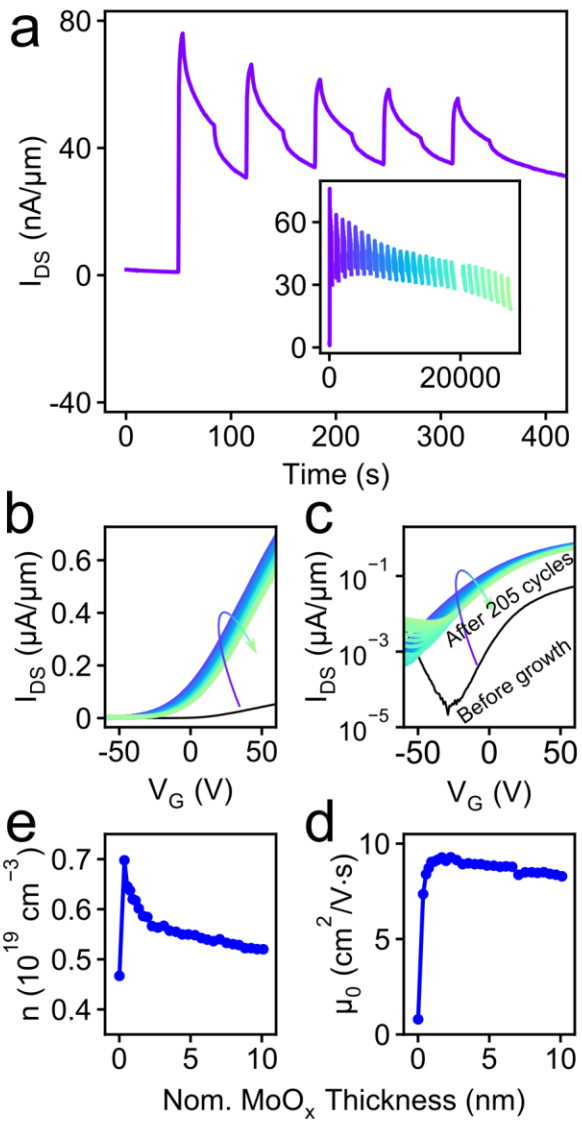

Figure 3. Evolution of electronic properties of $MoTe_2$ during ALD MoO_x growth. (a) Current density I_{DS} during the first five cycles of growth with V_G set at 55 V and V_{SD} set at 0.05 V. Inset: I_{DS} during the entire growth. Consecutive transfer curves collected every five ALD cycles for the entire growth in (b) linear) and (c) log scale. The increase in minimum current is partially due to an increase in leakage current (on the order of 10 nA) through MoO_x. Arrows indicate sequence of transfer curves. (d) Extracted carrier concentration n and (e) intrinsic mobility μ_0 show significant increases at the beginning of growth.

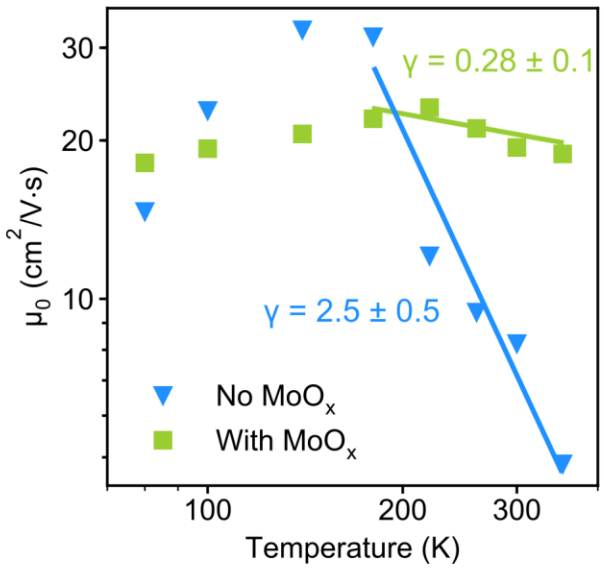

Figure 4. Variation of $MoTe_2$ mobility with temperature before and after MoO_x encapsulation. $\mu \sim T^{\gamma}$ dependence changes from $\gamma = 2.5$ to $\gamma = 0.28$ with MoO_x encapsulation. The error in γ is one standard deviation of the linear fit in the 180 K to 353 K range.

Supporting Information for

Operando studies of atomic layer deposition of dielectrics on transition metal dichalcogenide transistors

Ju Ying Shang,†⁺ Michael J. Moody,†⁺ Jiazhen Chen,‡ Sergiy Krylyuk,§ Albert V. Davydov,§ Tobin J. Marks, ‡,† Lincoln J. Lauhon†*

† Department of Materials Science and Engineering, Northwestern University, Evanston, IL 60208, United States
‡ Department of Chemistry, Northwestern University, Evanston, IL 60208, United States
§ Materials Science and Engineering Division, National Institute of Standards and Technology (NIST), Gaithersburg, Maryland 20899, United States

***E-mail: lauhon@northwestern.edu**

Contents

Supporting Information S1. Extraction of V_{Th} and μ_0 from Transfer Characteristics

Source-drain current during strong accumulation (when the transconductance was decreasing) was modeled with Equation (1) below[1,2], which assumed constant contact resistance and variable channel resistance,

$$I_D = \frac{W}{L} C_{gate}(V_G - V_{Th}) \frac{\mu_0}{1+\theta\cdot(V_G - V_{Th})} \cdot V_D \quad (1)$$

where I_D was the source-drain current and V_D was the applied source-drain bias, W and L were the width and length of the field-effect transistor (FET) channel, respectively. C_{gate} was the capacitance of the gate dielectric, V_G was the applied gate bias, V_{Th} was the threshold voltage, μ_0 was the intrinsic mobility of the channel, and θ was the mobility attenuation factor, which could be expressed as $\theta = (W/L)\mu_0 C_{gate} R_{contacts}$, where $R_{contacts}$ was the contact resistance.

To extract V_{Th} and μ_0, we assumed mobility to be carrier-concentration independent. In multilayer transition metal dichalcogenides (TMDs), carriers near the gate dielectric-TMD interface screen impurities at the interface, reducing scattering for carriers farther away from the interface[3]. Likewise, with multilayer TMDs, where carriers screened changes at the top atomic layer deposition (ALD) growth surface, gate capacitance could be assumed to be constant during oxide growth[4]. Using the parallel-plate approximation, the carrier concentration is $n_{2D} = C_{gate}(V_G - V_{Th})/e$, where e is the elementary charge. The 3D carrier concentration can then be determined as $n = n_{2D}/t$ where the thickness t can be measured by AFM.

During oxide growth, contact resistance changed minimally (**Figure S1a**). In order to fit source-drain current with less noise, contact resistance for each transfer curve was set as the average contact resistance of all the extracted $R_{Contact}$ from *operando* ALD growth. With variable temperature measurements (80 K to 353 K), mobility was extracted with constant contact resistance. Contact resistance varied within 1 kΩ (**Figure S1b**), which was on the same order of magnitude as errors associated with parameter extraction. To reduce fitting noise, contact resistance was set to be the average value of the extracted $R_{Contact}$ within the temperature range.

This analysis furthermore assumes that contacts are ohmic, and do not limit transport aside from the introduction of a series resistance. The devices measured here were confirmed to be ohmic by inspection of the linear output curves presented in **Figures S2 – S6**.

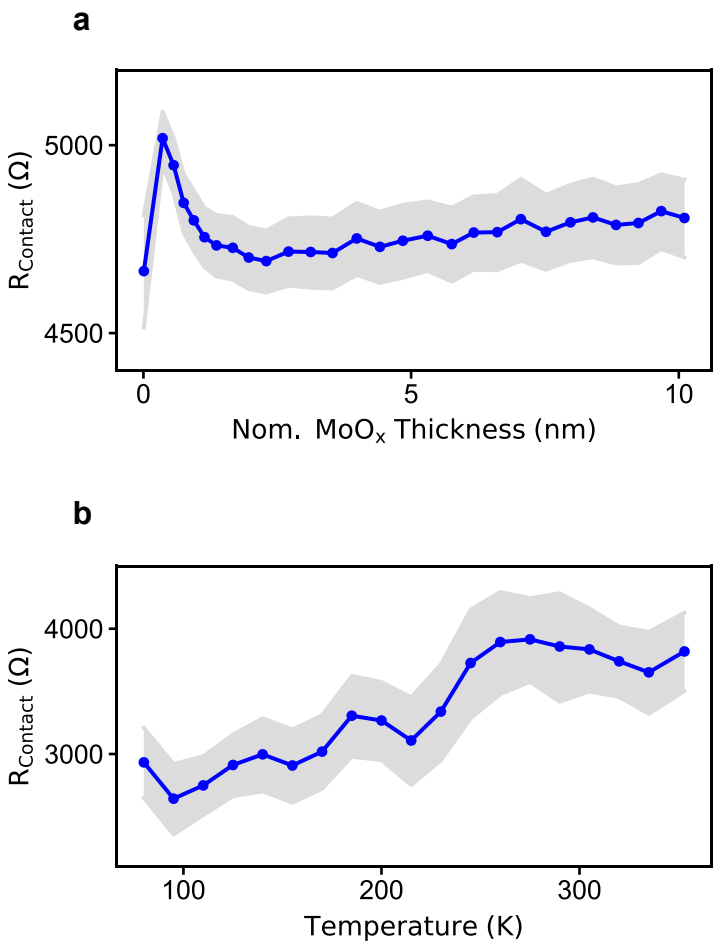

Figure S1. Variations in contact resistance. a, *Operando* contact resistance during MoO_x growth on unmasked MoS_2. Grey regions indicate three standard deviations for each extracted contact resistance. Due to the small variation in contact resistance throughout the growth, it is assumed constant for n and μ_0 extraction. **b**, Contact resistance for unmasked MoS_2 from 80 K to 353 K. Grey regions indicate three standard deviations for each extracted contact resistance. Due to the small variation in contact resistance with respect to temperature, it is assumed constant in μ_0 extraction.

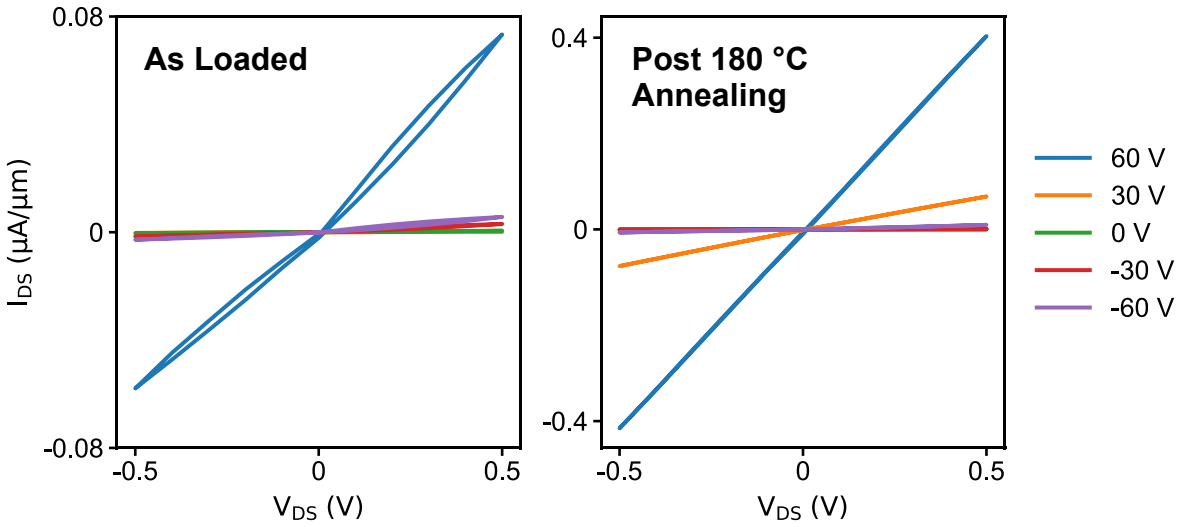

Figure S2. Output curves of $MoTe_2$ as loaded into the ALD chamber and post 180 °C annealing.

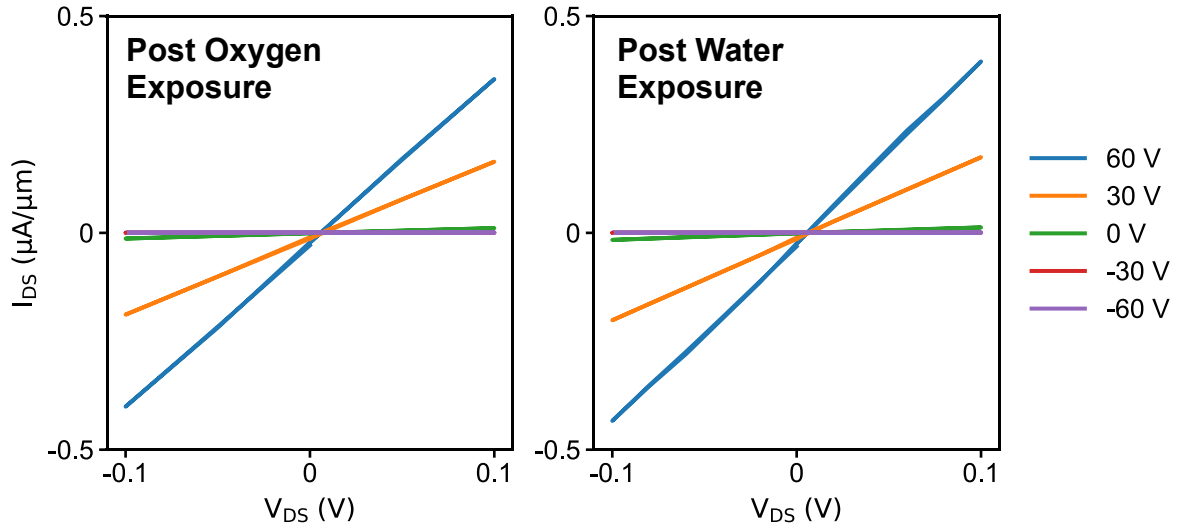

Figure S3. Output curves of $MoTe_2$ post oxygen and water exposure.

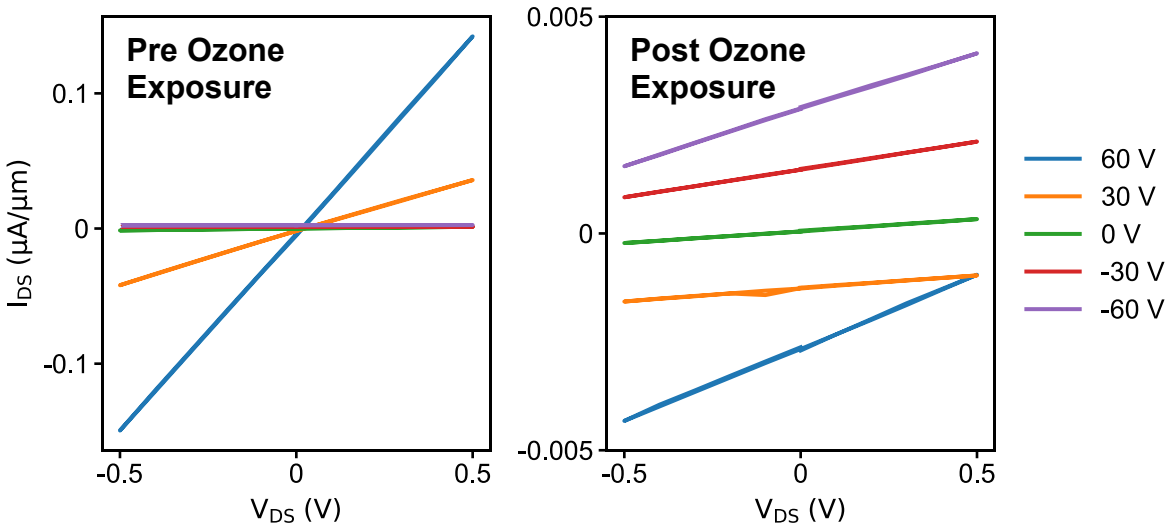

Figure S4. Output curves of $MoTe_2$ pre and post ozone exposure. With ozone exposure, leakage current increased, likely due to oxidation of $MoTe_2$ surface.

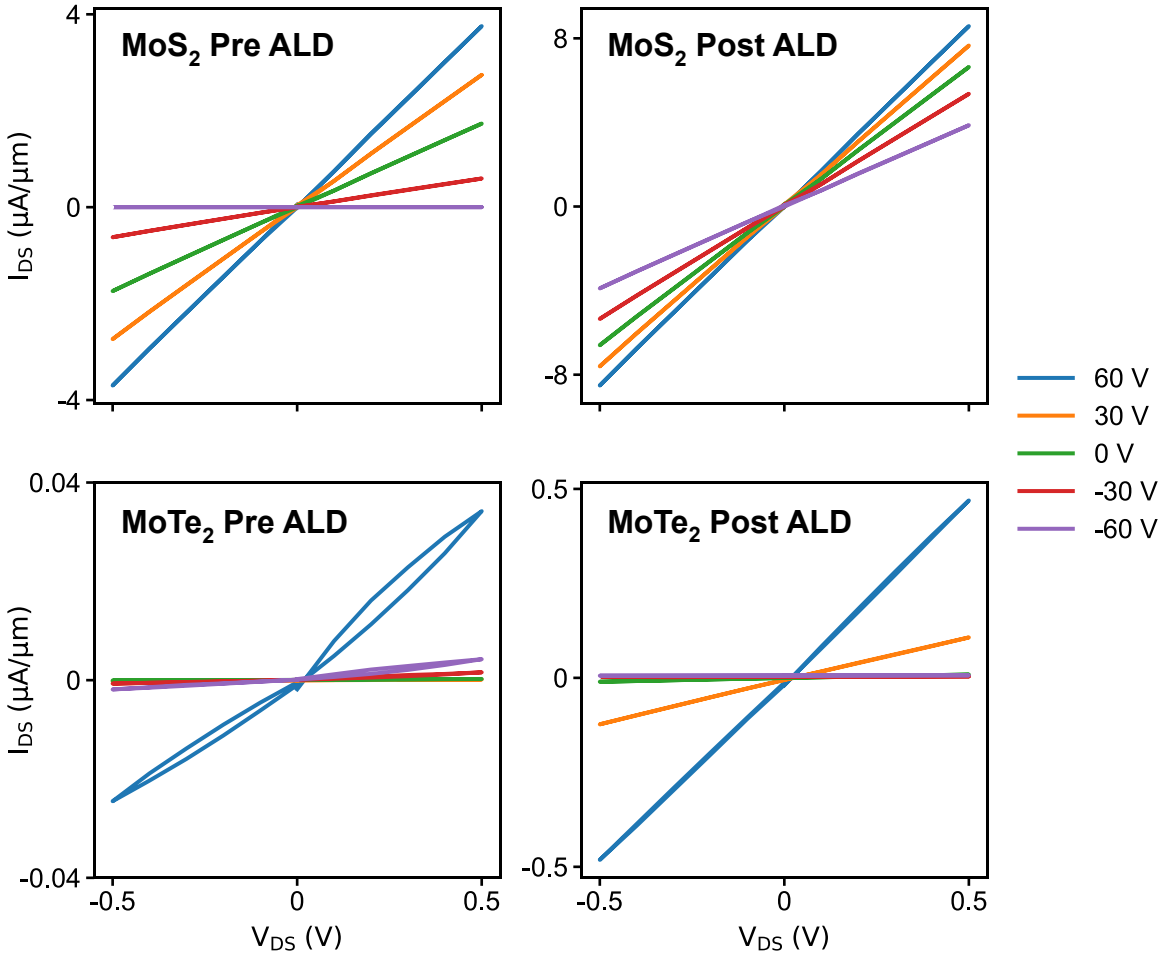

Figure S5. Output curves of MoS_2 and $MoTe_2$ pre and post ALD MoO_x/Al_2O_3 growth.

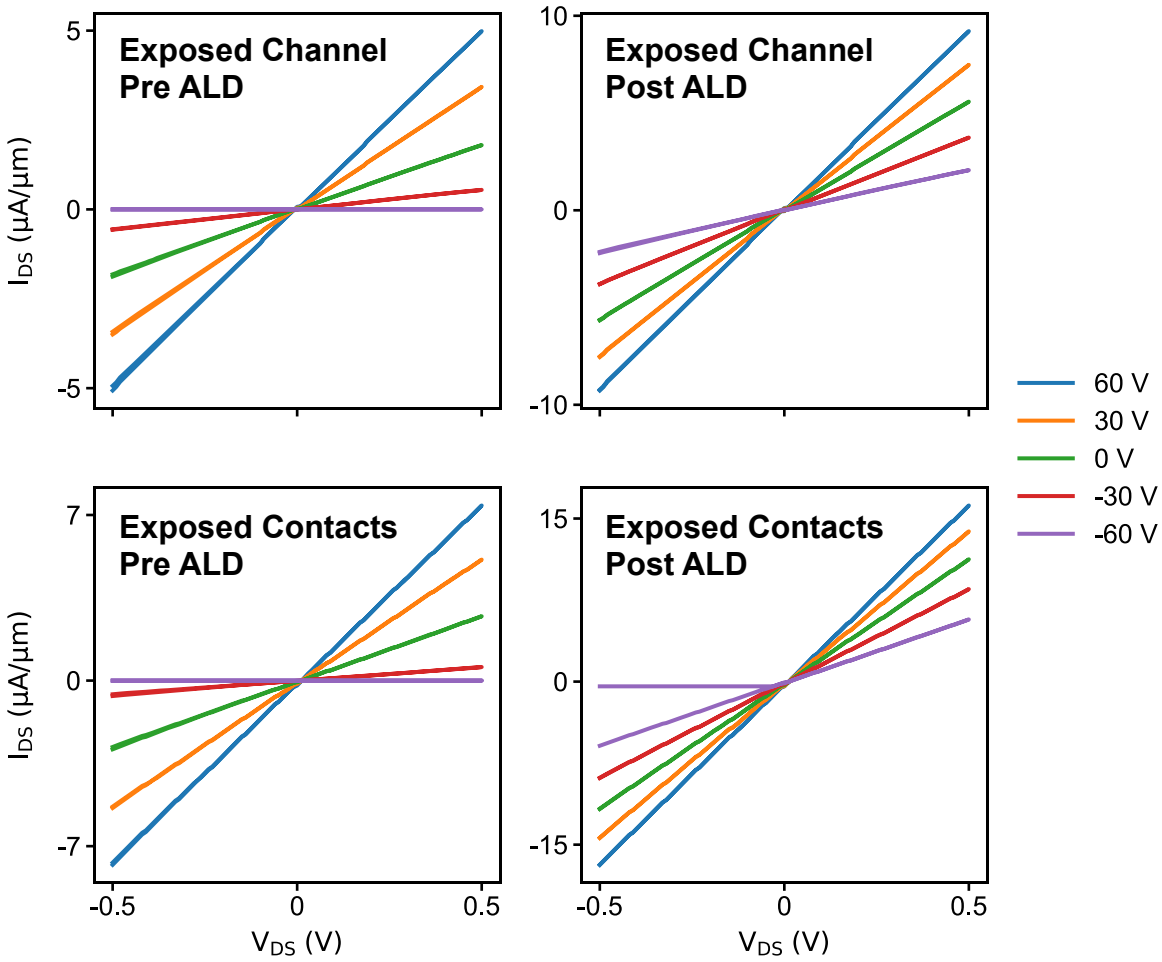

Figure S6. Output curves of Exposed Channel and Exposed Contacts MoS_2 pre and post ALD MoO_x/Al_2O_3 growth.

Supporting Information S2. Ozone Exposure

Operando measurements during exposure to O_3 (**Figures S7a, b**) show that O_3 modifies transport in $MoTe_2$ irreversibly, consistent with prior reports on partial oxidation forming MoO_3. After ozone exposure, electron mobility decreases by two orders of magnitude ((19 to 0.2) $cm^2/(V{\cdot}s)$) and electron concentration decreases from (5.0 to 2.5) $\times 10^{18}$ cm^{-3}, while hole mobility increases from a negligible value to 0.4 $cm^2/(V{\cdot}s)$. The original carrier concentration and mobility is not fully recovered after annealing, but rather the electron concentration remains 40 % lower and the mobility remains 89 % lower. The irreversibility is likely due to oxidation of $MoTe_2$ surface[5]. In real time, the first 3 ozone doses decrease current density (at a gate voltage of 0 V) as seen in **Figure S7a** top, while the subsequent doses (**Figure S7a** bottom) increase current density. This can be understood as a crossover from measuring electron depletion to hole accumulation as the majority carrier type changes in this ambipolar device

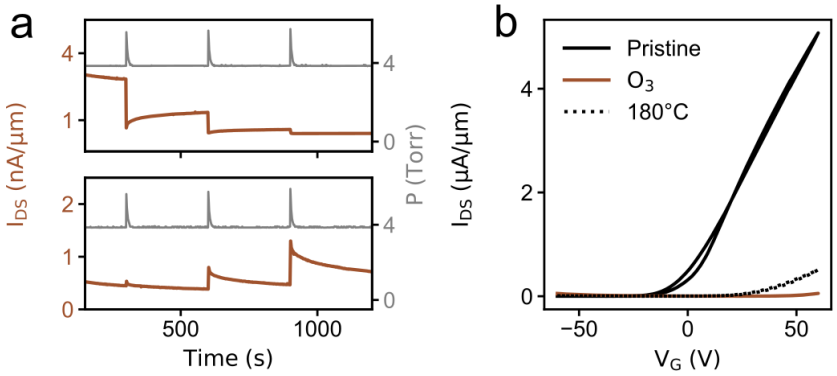

Figure S7. Effects of ozone exposure on $MoTe_2$ FET. a, When ozone is pulsed into the chamber, the continuously monitored channel current (at V_{DS} = 0.5 V and V_{GS} = 55 V) decreases with the initial 3 pulses (top) and increases with the subsequent 3 pulses. **b,** Electron mobility and concentration decrease after exposure, and are not recovered by baking at 180 °C.

Supporting Information S3. Channel current changes correlate with precursor introduction

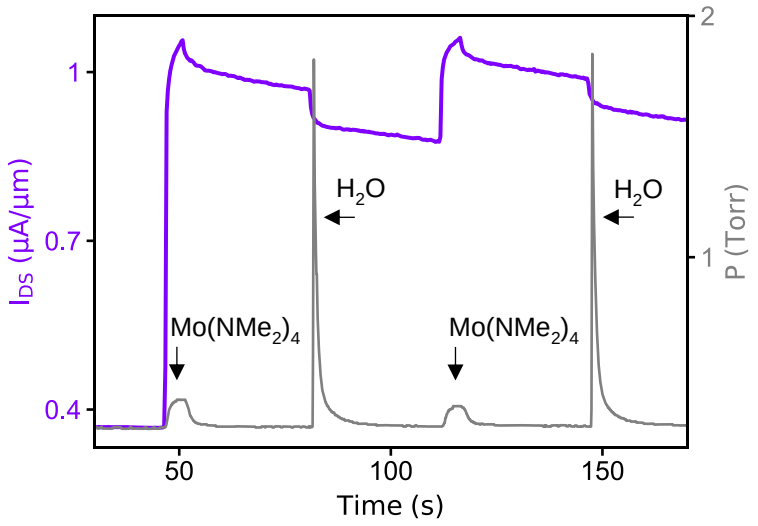

Figure S8. Time dependence of chamber pressure correlated with I_{DS} of unmasked MoS_2. The first pulse is $Mo(NMe_2)_4$, and the second pulse is H_2O. The two-step cycle alternates until ≈10 nm of MoO_x is grown.

Supporting Information S4. Calculation of mobility changes during initial cycles

Table S1. Table of values for percent increase calculation for unmasked MoS_2 FET.

	ALD Cycle 0	**ALD Cycle 1**	**ALD Cycle 5**	**% Inc**
n	1.2×10^{19} cm^{-3}	--	1.9×10^{19} cm^{-3}	60
μ_0	29 $cm^2/(V \cdot s)$	--	74 $cm^2/(V \cdot s)$	160
I_{DS}	0.37 μA/μm (forward sweep*) 0.37 μA/μm (backward sweep)	0.88 μA/μm	0.92 μA/μm	140⊥ 140⊥

* I_{DS} forward sweep comes from transfer curve measurement; backward sweep comes from I_{DS} real-time monitoring. Applies to Tables S1-S2. Tables S3-S4 only report I_{DS} from real-time monitoring.

⊥ % increase calculated between ALD Cycle 0 and ALD Cycle 1. ALD Cycle 5 I_{DS} is reported, but not used in calculations. Applies to Table S1-S4.

Table S2. Table of values for percent increase calculation for unmasked $MoTe_2$ FET.

	ALD Cycle 0	**ALD Cycle 1**	**ALD Cycle 5**	**% Inc**
n	4.7×10^{18} cm^{-3}	--	7.0×10^{18} cm^{-3}	50
μ_0	0.79 $cm^2/(V \cdot s)$	--	7.4 $cm^2/(V \cdot s)$	840
I_{DS}	4.7 nA/μm (forward sweep) 1.4 nA/μm (backward sweep)	31 nA/μm	30 nA/μm	560 2100

Table S3. Table of values for percent increase calculation for Exposed Channel MoS_2 FET.

	ALD Cycle 0	**ALD Cycle 1**	**ALD Cycle 5**	**% Inc**
n	1.2×10^{19} cm^{-3}	--	1.3×10^{19} cm^{-3}	0
μ_0	32 $cm^2/(V \cdot s)$	--	49 $cm^2/(V \cdot s)$	50
I_{DS}	27 μA/μm	38 μA/μm	40 μA/μm	40

Table S4. Table of values for percent increase calculation for Exposed Contacts MoS_2 FET.

	ALD Cycle 0	**ALD Cycle 1**	**ALD Cycle 5**	**% Inc**
n	1.3×10^{19} cm^{-3}	--	1.7×10^{19} cm^{-3}	30
μ_0	44 $cm^2/(V \cdot s)$	--	50 $cm^2/(V \cdot s)$	10
I_{DS}	34 μA/μm	48 μA/μm	50 μA/μm	40

Supporting Information S5. Mobility changes stop with deposition of Al_2O_3 Capping Layer

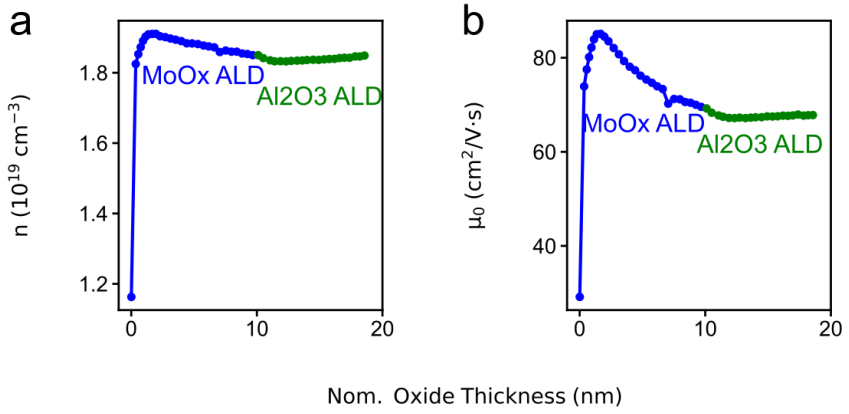

Figure S9. Evolution of carrier concentration and mobility during complete oxide deposition. Tracking both carrier concentration (a) and mobility (b) shows that the changes in both parameters slow as the capping Al_2O_3 is deposited and appear stable by the end of growth. This would be consistent with Al_2O_3 acting as a barrier, preventing further reaction or mass transport from the MoO_x film near the interface.

Supporting Information S6. *Operando* ALD with Masked FETs

Molecular adsorption and oxide growth at the near-contact region can affect transport properties[6]. To examine if the mobility increase noted previously is influenced by modulation at the contacts, we repeated the growth and *in situ* measurements with masked MoS_2 FETs. Electron-beam lithography and lift off were used to define a region of ALD-grown Al_2O_3 with thickness of 10 nm. For one geometry, shown schematically in **Figure S10a**, the contacts and near-contact regions are masked with Al_2O_3 and the channel is exposed ("exposed channel"). For a second geometry, shown schematically in **Figure S10b**, the majority of the channel is masked and the near-contact regions are exposed ("exposed contacts"). As fabricated, devices with both geometries show typical transport characteristics for MoS_2 FETs, ensuring the masked FETs are comparable to the unmasked ones. The same *operando* measurement parameters were used for masked FETs during a second MoO_x growth with the same two-step cycle and growth temperature.

With the exposed channel FET, we can isolate how the channel is being modulated during ALD growth. **Figure S10c** shows a negligible change in carrier concentration after the first five ALD cycles, and **Figure S10d** shows a 50 % increase in mobility. After the first cycle, **Figure S11b** shows a 40 % increase in current density. With the contacts masked, any change in the FET originates from changes to the channel. The increases in mobility and current density for the Exposed Channel FET provide evidence that the first ALD cycle reduces CI scattering in the channel, rather than primarily modulating transport at the contacts.

Operando measurements with the exposed contacts FET are consistent with this conclusion. Changes in carrier concentration and mobility originate from modulation of the contacts as well as changes in transport in the neighboring ca. 400 nm of exposed channel, but compared to the unmasked device, there will be a relatively larger contribution from any contact effects. **Figure S10e** shows a 30 % increase in carrier concentration after the first five ALD cycles, and **Figure S10f** shows a 10 % increase in mobility. After the first cycle, **Figure S11f** shows a 40 % increase in current density. Comparing this device (0.8 μm of channel exposed) to the exposed channel device (1.8 μm of channel exposed), it appears that MoO_x deposition on the near-contact region contributes proportionately less to the change in field effect mobility (by ca. 2 times), while contributing proportionately more to the shift in threshold voltage. Because both changes are more than two times smaller than the changes for the unmasked MoS_2 device (shown in **Figure 2** and **Table S1**), the near-contact region does not appear to play a disproportionate role in the evolution of transport with encapsulation, and contacts do not appear to limit charge transport in this regime.

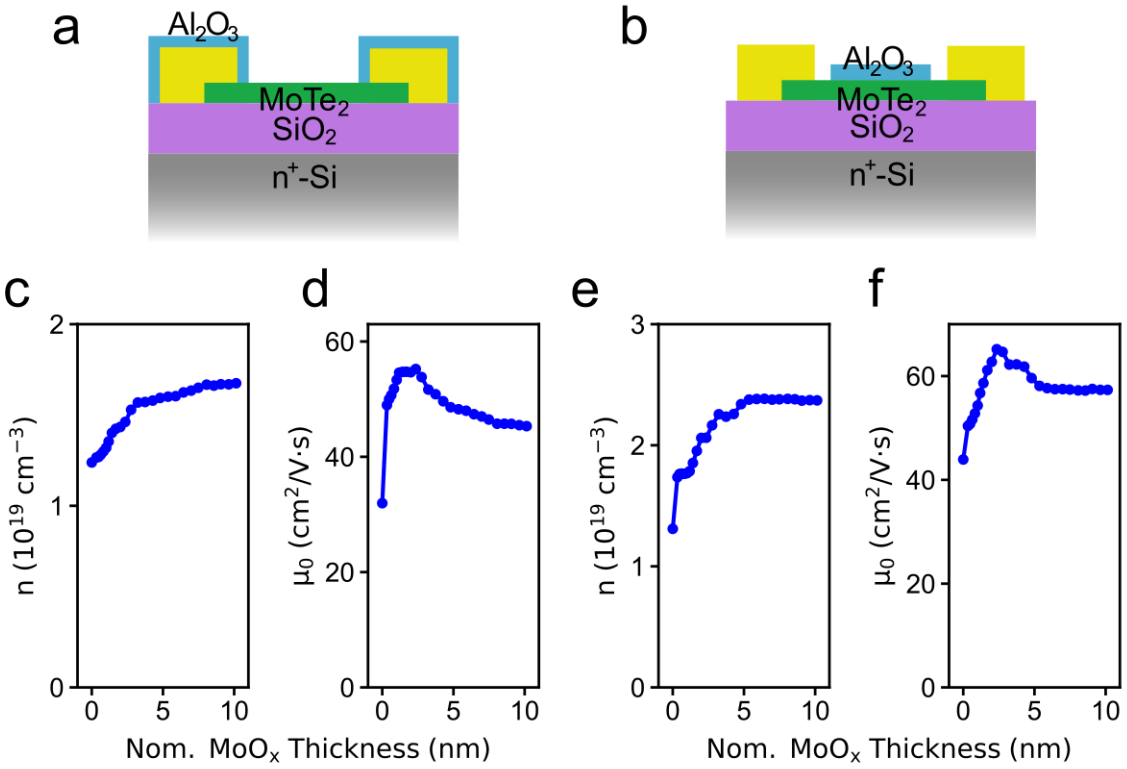

Figure S10. Evolution of electronic properties of masked MoS_2 FETs during ALD MoO_x growth. a, **b**, Schematics showing Exposed Channel FET (**a**) and Exposed Contacts FET (**b**). **c**, **d**, Extracted *n* (**c**) and μ_0 (**d**) for Exposed Channel FET. **e**, **f**, Extracted *n* (**e**) and μ_0 (**f**) for Exposed Contacts FET.

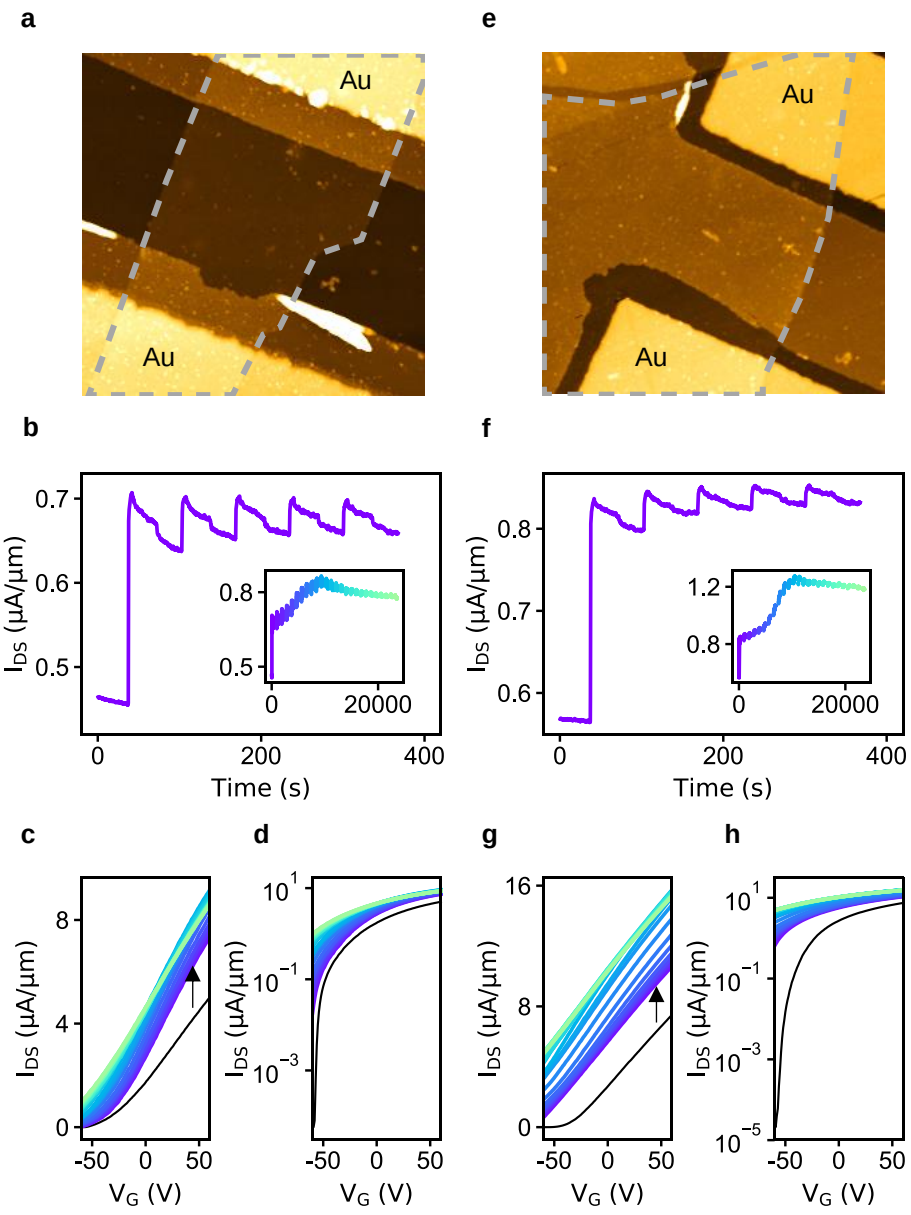

Figure S11. Evolution of electronic properties of Masked MoS_2 FETs during ALD MoO_x growth. a, AFM scan of Exposed Channel FET. The dashed line traces the MoS_2 flake. **b-d**, *Operando* measurements of Exposed Channel FET during growth. (**b**) shows I_{DS} during the first five cycles of growth. Inset: I_{DS} during the entire growth. Transport characteristic collected every five ALD cycle are shown in linear (**c**) and log (**d**) scale. Arrow indicate sequence of transfer curves. **e**, AFM scan of Exposed Contacts FET. The dashed line traces the MoS_2 flake. **f-h**, *Operando* measurements of Exposed Contacts FET during growth. (**f**) shows I_{DS} during the first five cycles of growth. Inset: I_{DS} during the entire growth. Transport characteristic collected every five ALD cycles are shown in linear (**g**) and log (**h**) scale. Arrows indicate the sequence of transfer curves.

Supporting Information S7. Variable-temperature transfer characteristics of an $MoTe_2$ FET

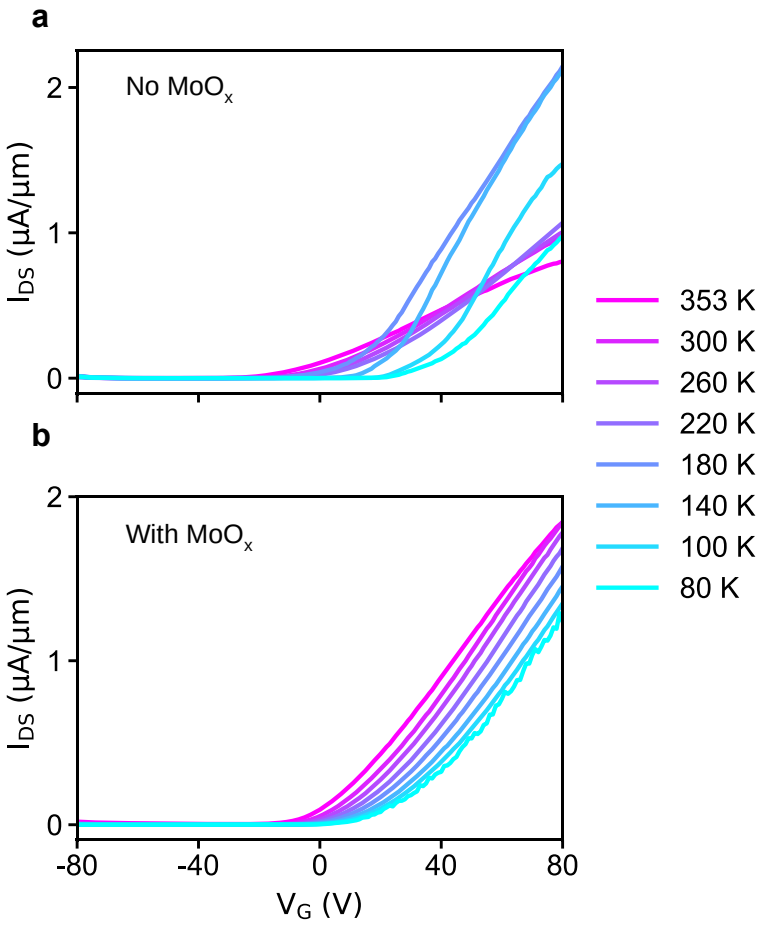

Figure S12. Transport characteristics of $MoTe_2$ FET at variable temperatures pre- (a) and post- (b) ALD MoO_x growth. Transfer characteristics were measured in high vacuum ($<1\times10^{-4}$ mbar) with V_{DS} = 0.1 V.

Supporting Information S8. Device dimensions, experiments, and figures

Table S5. Table of Devices.

Device #	Channel Material	Length (μm)	Width (μm)	Thickness (nm)	Figure #	Measurement/Experiment
Te18_Dev2	$MoTe_2$	4.0	2.7	8	Figures 1cd, S2	Oxygen and water exposure real-time monitoring
Te12_Dev2	$MoTe_2$	5.0	2.5	9	Figures S4, S7a	Ozone exposure real-time monitoring
Te11_Dev1	$MoTe_2$	3.9	3.5	5	Figures 1ef, S3	Oxygen and water exposure transfer curve measurements
Te18_Dev1	$MoTe_2$	2.0	2.5	8	Figure S7b	Ozone exposure transfer curve measurements
S-Te1_Dev1	MoS_2	4.0	6.1	7[#]	Figures 2, S1a, S5, S8	MoO_x ALD Growth 1 MoS_2 Experiment
Te12_Dev1	$MoTe_2$	4.3	2.2	7	Figures 3, S5	MoO_x ALD Growth 1 $MoTe_2$ Experiment
S4_Dev1	MoS_2	3.0	2.0	5	Figures S10cd, S11abcd, S6	MoO_x ALD Growth 2 Exposed Channel Experiment
S5_Dev2	MoS_2	3.0	2.4	5	Figures S10ef, S11efgh, S6	MoO_x ALD Growth 2 Exposed Contacts Experiment
Te42_Dev2	$MoTe_2$	3.0	2.2	8	Figures 4, S12	MoO_x ALD Growth 3 variable temperature transfer curve measurements
Te35-MoS2_Dev2	MoS_2	3.0	4.0	8[#]	Figure S1b	Variable temperature transfer curve measurements

[#] Thicknesses estimated from S-Te1_Dev2, with a thickness of 6 nm.

References

1 Schroder, D. K. Semiconductor Material and Device Characterization. 489-499 (2006).

2 Xu, Y., Minari, T., Tsukagoshi, K., Chroboczek, J. A. & Ghibaudo, G. Direct evaluation of low-field mobility and access resistance in pentacene field-effect transistors. *Journal of Applied Physics* **107**, doi:10.1063/1.3432716 (2010).

3 Li, S. L. *et al.* Thickness-dependent interfacial Coulomb scattering in atomically thin field-effect transistors. *Nano Lett* **13**, 3546-3552, doi:10.1021/nl4010783 (2013).

4 Liu, Y. *et al.* Toward barrier free contact to molybdenum disulfide using graphene electrodes. *Nano Lett* **15**, 3030-3034, doi:10.1021/nl504957p (2015).

5 Zheng, X. *et al.* Controlled Layer-by-Layer Oxidation of MoTe2 via O3 Exposure. *ACS Appl Mater Interfaces* **10**, 30045-30050, doi:10.1021/acsami.8b11003 (2018).

6 Duran Retamal, J. R., Periyanagounder, D., Ke, J. J., Tsai, M. L. & He, J. H. Charge carrier injection and transport engineering in two-dimensional transition metal dichalcogenides. *Chem Sci* **9**, 7727-7745, doi:10.1039/c8sc02609b (2018).